Study of Galvanic Corrosion Potential of NSM Titanium Reinforcing Bars

Shawn Platt[1] and Kent A. Harries[2]

Abstract

The use of titanium as a near surface mounted (NSM) reinforcing material has been proposed. This study assesses the effects of coupling 6Al-4V titanium and ASTM A615 black steel in NSM applications. In order to place the use of titanium in context, duplicate specimens having stainless steel and CFRP NSM bars are also tested. Sixty-two concrete prisms were tested, each having a single embedded #4 ASTM A615 (Grade 60) black steel bar. A 12.7 mm diameter titanium (Ti), CFRP or 2205 stainless steel (SS) NSM bar is embedded along one side of the concrete prism into NSM 'slots'. Specimens were conditioned in a cyclic temperature and humidity environment for two years during which half-cell potential (ASTM C876) and macrocouple current (ASTM G102) were monitored. Following conditioning, all steel bars were removed and mass loss due to corrosion determined. The comparison of interest in this study is as follows: *does the presence of titanium accelerate or result in greater steel corrosion than other materials coupled with mild reinforcing steel; that is, does a more aggressive galvanic cell develop?* For the conditions tested, corrosion was present in all specimens. There was no evidence that the presence of 6Al-4V titanium reinforcing bars in close proximity to (or in electrical contact with) A615 steel reinforcing bars results in any change in the rate or nature of corrosion.

Keywords: concrete; corrosion; galvanic corrosion; reinforcing bars; titanium

---

[1] PhD candidate, University of Pittsburgh

[2] Bicentennial Board of Visitors Faculty Fellow and Associate Professor, University of Pittsburgh, kharries@pitt.edu

Introduction

Titanium reinforcing bars for concrete rehabilitation have been proposed and demonstrated in laboratory tests and in a single field application (Higgins et al. 2015 and 2017; Adkins and George 2017). The demonstrated application was the near-surface mounting (NSM) of smooth bar titanium 'staples' – straight bars having a 90 degree bend at either end to affect anchorage. The primary advantage of titanium is its corrosion resistance permitting the reduced cover inherent in an NSM repair. The present paper is part of a large study investigating specific aspects of the use of titanium as a concrete reinforcing material (Platt 2018).

It is proposed that titanium reinforcing bars may have applications in concrete and masonry repair (Adkins and George 2017), particularly in unique environments and in connection with historic structures since titanium is noncorroding. Nonetheless a number of performance parameters in relation to titanium reinforcing bars and their integration into new or existing construction remain. In particular, titanium is known from the marine industry to drive galvanic corrosion in steel (Bomberger et al. 1954). If this also occurred in the passivating environment of concrete, it would be 'show stopper' for the use of titanium reinforcement in the presence of steel reinforcement. This paper reports the findings of a comparative study of the galvanic corrosion potential of titanium embedded in concrete.

Galvanic Corrosion in Steel-reinforced Concrete

Galvanic corrosion is a primary cause of corrosion affecting steel-reinforced concrete. Galvanic corrosion in steel-reinforced concrete is more likely to play an important role in the corrosion of large areal structures such as bridge decks and arises from differences in aeration (oxygen), alkalinity (carbonation) or salt (chloride) concentration; all resulting in uneven passivation of the reinforcement (Gulikers and Schlangen 1996). The extensive use of de-icing salts is believed to result in the disproportionate instance of damage to bridge structures attributed to galvanic corrosion in North America (Song and Shayan 1998). Nonetheless, there are relatively few systematic studies of galvanic corrosion in steel-reinforced concrete.

Extensive issues with corrosion have led some to use stainless steel reinforcing bars in susceptible structures. Due to the cost of stainless steel, it is often only used for top-slab reinforcing while conventional 'black' steel is used elsewhere. This use of dissimilar materials raises the potential for galvanic corrosion to accelerate the corrosion of the black steel in the system. A number of studies have investigated this effect. Provided both the black and stainless steels remain passive, the use of stainless steel has not been found to increase the risk of corrosion of the black steel (Perez-Quiroz et al. 2008; Bertolini and Pedeferri 2002; Knudson and Skovsgaard 2001; Klinghoffer et al. 2000; Cochrane 1999). Hope (2001) concluded that although corrosion of black steel would occur in a galvanically-coupled system when the concrete is contaminated with chlorides or carbonated, the rate of corrosion would not be appreciably different than if black steel alone were present. Indeed, Qu et al. (2003) and Broendby (1999) concluded that coupling black steel and stainless steel results in lower corrosion rates than coupling black steel in a chloride-laden environment. Webster (1997) and Seibert (1998), on the other hand, indicate that galvanic corrosion will take place when stainless and black steel are electrically coupled and recommend that these materials be electrically isolated from one another. Stainless steel reinforcing steel is accepted as an alternative reinforcement in highly corrosive environments and by most bridge owners in North America.

Similar questions of the potential for galvanic corrosion are raised when using carbon fibre reinforced polymer (CFRP) composite materials in repair of steel-reinforced concrete. ACI 440.2R (2017) recommends that in order to mitigate the possibility of galvanic corrosion, steel and CFRP not be in contact. PCA (1970) recommends that nonferrous metals (copper, zinc, aluminium and lead) in contact with concrete should be electrically isolated from the reinforcing steel. In the presence of chlorides, galvanic corrosion is also likely for nickel and cadmium coated steel reinforcement (PCA 1970).

Galvanic Corrosion of Steel Coupled with Titanium

Most data on galvanic corrosion with titanium relates to the materials in a marine environment. A low-velocity, poorly aerated sea-water environment is not dissimilar to the environment in chloride-laden

concrete. Coastal steel-reinforced concrete structures, in addition to those subject to de-icing salts, exhibit significant amounts of galvanic corrosion.

In most environments, titanium will be the cathodic member of a galvanic couple. In terms of voltage potential in moving seawater versus a saturated calomel reference electrode, titanium has a potential of 0V; mild steel has a potential of -0.65V, making the steel the active anode (Laque 1975). By comparison, stainless steel has a potential near -0.5V when active.

In a marine environment, titanium has been shown to have an accelerating effect on the corrosion rate of mild steel when galvanically connected (Cotton and Downing 1957; Bomberger et al 1954). If the surface area of titanium is small in relation to the area of steel, the accelerating effect is negligible. However, if the area of the titanium greatly exceeds the area of steel the corrosion rate has been observed to increase over 500% (Cotton and Downing 1957).

Objective of Study

The objective of the reported study is to assess the effects of coupling titanium and black steel in typical concrete. The titanium is alternately 1) embedded in the concrete; 2) 'potted' in an epoxy resin prior to embedment in concrete; or 3) 'potted' in a cementitious repair mortar prior to embedment in concrete. The potted specimens are intended to better replicate conditions in a repair scenario in which the titanium will be used as NSM reinforcement. In order to place the use of titanium in context, duplicate specimens having stainless steel and CFRP reinforcing bars are also tested.

Test Description

Specimens

Sixty-two 152 x 152 x 152 mm concrete prisms were formed as summarized in Table 1. Each prism has a single #4 (12.7 mm diameter) black steel bar (ASTM A615 Grade 60) embedded a distance *d* from the concrete surface to which the NSM 'repair' is made. A 12.7 mm diameter titanium (Ti), CFRP or 2205 stainless steel (SS) NSM bar is embedded along one side of the concrete prism into NSM 'slots' having dimensions recommended by ACI 440.2R-17 for NSM CFRP (Figure 1). The NSM bars were 'potted' in advance (rather than having to cut and install all NSM bars following concrete placement).

Additional specimens having titanium NSM strips (Tis) of the same cross sectional area (129 mm^2) were also tested since such strips reduce installation cost in NSM applications. In the strip applications, the width of the slot was only $2.5a_b$, rather than the $3a_b$ shown in Figure 1. All bar specimens are shown, prior to placement in concrete, in Figure 2a. Specimens following placement of concrete are shown in Figure 2b. Control specimens having the NSM and black steel bars electrically coupled (Figure 3c) and specimens having no NSM bar were also prepared. The detailed test matrix is provided in Table 1. Two replicates of each specimen were made.

Materials

Concrete – a commercially available premixed concrete was used. This mix reports a cement (Type I/II) content of 20%. 4.55 L water was mixed per 80 lb bag of concrete resulting in a water/cement (*w/c*) ratio of 0.63. In order to increase the conductivity of the concrete, thereby accelerating any galvanic corrosion present (e.g. Mangat and Elgarf 1999; Nossoni et al. 2015), 252 g per bag of concrete of laboratory grade (95% w/w) calcium chloride dihydrate (Fisher Scientific S25221A) was dissolved (prior to concrete mixing) into the mix water. This is equivalent to 4.28% $CaCl_2$ by weight of cement based on industry-standard $CaCl_2$ flake (77%) equivalence. Such an approach is intended to replicate chloride-laden concrete which may be typical of an older bridge or parking structure or a structure located in a sea water environment.

Specimens were cured in a standard laboratory environment for more than 28 days prior to beginning conditioning. At 28 days, standard compression (ASTM C39) tests were performed in order to quantify the concrete used. The compressive strength, f_c' = 29.5 MPa (COV = 0.10) and the modulus, E_c = 22.2 GPa (COV = 0.04).

Black Steel – ASTM A615 Grade 60 #4 bars, having a nominal diameter of 12.7 mm and area of 129 mm^2, were used. The yield strength, f_y, was experimentally determined to be 476 MPa.

Titanium bars – smooth 6Al-4V titanium bars having a diameter of 12.7 mm were used. The yield strength, f_y, was experimentally determined to be 1019 MPa.

Titanium strips – 25.4 x 6.4 mm 6Al-4V titanium strips were provided by the manufacturer. In order to have the same cross sectional area as the bars, these were machined to a width of 5.1 mm for use in this study. The yield strength, f_y, was experimentally determined to be 931 MPa.

CFRP – commercially available sand-coated CFRP reinforcing bars having a nominal diameter of 12.7 mm were used. These bars have a guaranteed tensile strength of 2070 MPa and tensile modulus of 124 GPa.

Stainless Steel – Grade 2205 Duplex #4 bars, having an experimentally determined yield strength of 579 MPa were used.

NSM Epoxy – a commercially available two-part structural adhesive, based on a combination of epoxy resins and proprietary filler was used. The adhesive is commonly used to bond structural reinforcement in NSM applications.

NSM cementitious grout – a commercially available one part flowable shrinkage compensating cementitious grout was used. The grout is commonly used in concrete repair applications and to bond steel reinforcement anchors.

Conditioning Protocol

Following 35-days laboratory curing, specimens were placed in a covered water-filled plastic tank (Figure 3b). The specimens were supported on a non-corrosive, non-conductive GFRP rack above the water level (Figure 3a). A thermostat-controlled tank heater[3] was used to raise the water temperature and therefore the temperature/humidity in the covered tank. When heated and covered, air temperature surrounding the specimens varied between 29ºC and 35ºC and relative humidity (RH) was typically logging 99.9%. When unheated and not covered, the specimens were in an air-conditioned ambient laboratory environment in which temperature remained approximately 21±2ºC and RH varied as low as 25%. The environment was typically cycled on a 1-2-1-3 day cycle as shown in Table 2. Conditioning began April 7 2015 and lasted

[3] The tank heater turned on at 27ºC and shut off at 49ºC water temperature resulting in variation of conditioning environment temperature and RH as indicated.

746 days (April 26 2017). The temperature and humidity in the tank was monitored on an hourly basis using an Extech 42280 temperature/RH logger (seen in Figure 3c). A typically weekly log is shown in Figure 4.

Specimen Monitoring

Two series of tests were conducted on a regular basis. Tests were conducted on a twice-weekly basis early in the conditioning protocol and on a bi-weekly basis later. All tests were conducted following a period of 24h drying (i.e., typically Tuesday or Friday mornings prior to the tank being recovered and the heater reengaged as indicated in Table 2).

Half-cell potential Using the Potential Difference Technique (ASTM C876 10.3)

Half-cell potential tests were conducted using a James Instruments Cor-Map System having a copper-in-saturated copper sulphate solution ($Cu\text{-}CuSO_4$) reference cell. By connecting a high impedance voltmeter (variable impedance from 10 MΩ to 200 MΩ; compliant with ASTM C876 supplied with Cor-Map System) between the reinforcing steel (the A615 bar in all cases) and a reference electrode placed on the concrete surface, a measurement can be made of the half-cell potential at the location of the reference cell. This is an indication of the probability of corrosion activity in the steel in the vicinity of the reference cell. ASTM C876 provides the following guidance in interpreting results of this test.

- For readings that are more negative than -350 mV there is a 90% chance of active steel corrosion.
- For readings between -200 and -350 mV the results are inconclusive.
- For readings that are more positive than -200 mV there is only 5% chance of active steel corrosion.
- Readings that have relatively high negative values with little variance in time may indicate that corrosion is possible but that oxygen availability is very limited impeding the corrosion process.

Macrocouple Current (based on ASTM G102)

Direct measurement of current between the embedded A615 steel bar and NSM bar was made using a Keithley 485 Autoranging Picoammeter. The measured current is an indirect measure of the average rate

of corrosion present in each specimen. Values of measured current may be compared to assess relative rates of corrosion. Faraday's law may be used to estimate the theoretical corrosion penetration rate or mass loss rate (ASTM G102) which vary in proportion to measured current.

Measurement of Reinforcing Bar Mass Loss

Following the conditioning period, all steel bars were recovered and mass loss due to corrosion determined. The following procedure was carried out to determine an average mass loss. All bars were sand-blasted (garnet abrasive with a Moh's hardness of 7.5) to remove adhering concrete and corrosion product. The bars were cut to their 152 mm embedment length and weighed. The masses were compared to the mass of uncorroded control specimens cut from the same reinforcing bar. The average mass of an uncorroded bar was 0.89 g/mm. Using the lineal mass as the control allowed the tested bars to be cut smaller to isolate corrosion pits or highly localised corrosion. These shorter samples having greater corrosion present yield greater values of mass loss. As the length of sample decreases, the mass loss calculation is increasingly a better estimation of cross section loss which, more than mass loss, is critical to reinforcing bar tension capacity.

Test Results

Prior to Conditioning

Initial 'zero' readings were made 7 April 2015 prior to any conditioning cycles. The half-cell potential data indicated the *potential* for steel corrosion; that is, the black steel was not passivated in the chloride-laden concrete environment. The average reading for all specimens was -400 mV (COV = 0.13) with maximum and minimum recorded values of -269 and -517 mV, respectively. As expected, there was no statistically significant variation based on material (Ti, Tis, CFRP or SS) or NSM embedment material (concrete, epoxy or grout) at the initiation of conditioning.

Macrocouple current data in the previously unconditioned specimens is summarized in Figure 5. In the previously unconditioned and non-corroding specimens, the current varied seven orders of magnitude – from 70 pA (essentially negligible) to 41.7 μA. The macrocouple data indicates that the epoxy NSM material is an effective electrical insulator; the macrocouple current in specimens with epoxy NSM

embedment did not exceed 0.1 μA, representing a statistically significant variation from concrete ($p = 0.01$) and grout ($p = 0.03$) embedment. A less significant variation ($p = 0.07$) was observed between concrete and grout embedment although this is skewed by consistently high results for the stainless steel embedded in grout (see Figure 5). Curiously, despite their epoxy-rich exterior coating, the CFRP bars did not appear to be electrically insulated and exhibited macrocouple currents similar to the other materials when embedded in the same NSM material. It can be seen in Figure 5 that the Ti strip material exhibited uniformly greater macrocouple current than the Ti bars. This may partially result from the 53% greater surface area of the strips compared to the bars (Table 1).

During Conditioning

Beyond establishing the high probability for corrosion of the black steel to develop, half-cell measurements are less useful in the time domain for small specimens. The cyclic wetting and drying washes/leaches the surface chlorides out of the relatively small specimens resulting in the potential approaching a steady state (Poursaee 2011). Nonetheless, the average measured half-cell potential remained below -248 mV over the two-year conditioning programme as seen in Figure 6.

Macrocouple current increased with time in most all specimens. This indicates that, in general, some degree of corrosion is occurring. Figure 7 repeats Figure 5 showing the macrocouple readings at the end of conditioning. Macrocouple current was similar for concrete and grout embedment and significantly lower for epoxy embedment. The epoxy initially serves as an insulator, mitigating the galvanic cell. However, the epoxy also degrades in an aggressive hygrothermal environment, becoming more permeable; this results in greater variance in the epoxy-embedded data. Complete time histories of all data are found in Platt (2018).

A statistical analysis using the Bonferroni correction (at 95% confidence interval) was carried out on the macrocouple data. Due the small sample size for each variation, only the apparent trends can be described:

1. Galvanic cells including stainless steel bars exhibited greater macrocouple current than the other materials. Titanium bars, strips and CFRP bars did not differ from one another. Based on this

observation, the stainless steel bars were checked for corrosion (which would lower their potential) – none was observed.

2. Epoxy embedment resulted in lower macrocouple current as the epoxy serves as an insulator. The grout embedment resulted in higher macrocouple currents. This is believed to result because the grout used is likely to have a greater porosity than the surrounding concrete.
3. In the small specimens, the separation between bars (dimension *d*) had no significant effect on results.
4. An analysis dividing results into subsets of the 746-day conditioning period showed that change in macrocouple was more significant in the first six months of conditioning (Platt 2018). This result would appear to reflect the observation of the increasing (less negative) half-cell potential described previously.

Following Conditioning

Following 434 days of conditioning (14 June 2016), small radial cracks emanating from the A615 bar were observed on some specimens. These are an indication of volumetric expansion of the bar resulting from corrosion. Three specimens were removed to determine the average mass loss over the 152 mm bar embedment at the time radial cracking appeared; this was determined to range from 2% to 4.7% mass loss.

Mass loss was determined for the remainder of the specimens following 746 days of conditioning (Figure 8). Corrosion was observed in all specimens. Control specimens having no galvanic cell exhibited approximately 5.8% average mass loss after two years conditioning (Table 3). None of the galvanic cells (Fe-Ti bar, Fe-Ti Strip, Fe-SS, Fe-CFRP) exhibited statistically significant different behaviour from each other or the control. 2205 duplex stainless steel exhibited statistically poorer behaviour than Ti strips ($p = 0.01$) and CFRP ($p = 0.09$). The presence of titanium in the galvanic cell was not detrimental to corrosion performance as compared to industry-accepted reinforcing materials: stainless steel and CFRP.

Based on visual analysis, the greatest corrosion pits for each bar were identified and the mass loss determined for a shorter (12.6 mm) specimen encompassing the pits determined. The ratio of pit mass loss to average mass loss (Table 3) is an additional measure that can be integrated into remaining life

calculations (Gonzalez et. al. 1995). The values observed in this study are consistent with similar such ratios reported in the literature.

Mass loss of electrically connected bars

The electrically connected specimens (see Table 1 and Figure 3) should ensure a galvanic cell develops if one was likely. There was no statistical difference between the performance of these specimens and those in which the circuit is closed through embedment only. This result reinforces the conclusion that no additional galvanic corrosion process was present in the test program and that the presence of titanium has no different effects than stainless steel or CFRP.

Conclusion

Galvanic corrosion cells were induced in chloride-laden steel-reinforced concrete specimens. The specimens each contained a "black" steel (ASTM A615) reinforcing bar anode electrically coupled through concrete embedment with titanium, stainless steel or CFRP bar cathodes. Based on the galvanic series, titanium would be expected to result in a more aggressive galvanic cell when coupled with steel than would stainless steel or CFRP. The objective of this study was to assess whether the presence of titanium reinforcement accelerates or otherwise results in greater steel corrosion than stainless steel or CFRP reinforcement when electrically coupled with mild reinforcing steel.

For the conditions tested, modest corrosion – about 5.5% average mass loss over two years – was present in all specimens including those not having a galvanic cell present. Pitting corrosion, resulting in more significant steel cross sectional area loss was observed in all cases. The pitting observed for the titanium cathodes was no different than the control case. Despite their epoxy-rich sand-coated exterior, the CFRP bars exhibited macrocouple currents only slightly lower than those of stainless steel or titanium; the resulting corrosion of the black steel anode in these cases was reduced although not mitigated and pitting was less significant. Pitting of the "black" steel anode in those specimens having 2205 duplex stainless steel cathode bars was greater: evidence of an active galvanic corrosion effect.

There was no evidence that the presence of 6Al-4V titanium reinforcing bars in close proximity to (or in electrical contact with) A615 steel reinforcing bars resulted in any change in the rate or nature of

corrosion. Thus there is no impediment from the perspective of potential galvanic corrosion performance to the use of titanium bars as near surface reinforcement (NSM).

Macrocouple current was similar for concrete and grout embedment of the cathodic material and significantly lower for epoxy embedment. The epoxy initially serves as an insulator, mitigating the galvanic cell. However, the epoxy is believed to have degraded in the aggressive hygrothermal environment, becoming more permeable as the test progressed resulting in more variable data for the epoxy-embedded cathodes. In this study macrocouple current was slightly greater in the specimens in which the cathodes were embedded in cementitious grout. This is believed to reflect the greater porosity of the grout as compared to the host concrete.

This study, while limited, illustrates a few potential issues associated with near surface mounted (NSM) reinforcement: NSM applications using metallic bars run the risk of developing a galvanic corrosion cell which could accelerate active corrosion of the existing "black" steel. Embedding NSM bars in a durable epoxy matrix helps to mitigate this risk by partially electrically insulating the bars. CFRP bars, having an epoxy outer layer, are also preferred as these are less electrically active than their metallic counterparts.

Acknowledgement

The research presented was sponsored by the Perryman Company. The findings and conclusions reported in this paper reflect the opinion of the authors and are not necessarily those of the Perryman Co. The contributions of Salit Specialty Rebar (Niagara Falls NY) and Hughes Brothers (Seward NE) are gratefully acknowledged.

References Cited

ACI 440.1R-15 *Guide for the Design and Construction of Structural Concrete Reinforced with FRP Bars*, American Concrete Institute.

ACI 440.2R-17 *Design and Construction of Externally Bonded FRP Systems*, American Concrete Institute.

ACI 440.7R-10 *Guide for the Design and Construction of Externally Bonded Fiber-Reinforced Polymer Systems for Strengthening Unreinforced Masonry Structures*, American Concrete Institute.

Adkins, J. and George, W. (2017) Titanium Finds a Home in Civil Engineering, *Concrete International*, December 2017, pp 51-55.

ASTM A615-16 *Standard Specification for Deformed and Plain Carbon-Steel Bars for Concrete Reinforcement*, ASTM International.

ASTM C39-16 *Standard Test Method for Compressive Strength of Cylindrical Concrete Specimens*, ASTM International.

ASTM C876-09 *Standard Test Method for Corrosion Potentials of Uncoated Reinforcing Steel in Concrete.* ASTM International.

ASTM G102-10 *Standard Practice for Calculation of Corrosion Rates and Related Information from Electrochemical Measurements*, ASTM International.

Bertolini and Pedeferri (2002) Laboratory and Field Experience on the Use of Stainless Steel to Improve Durability of Reinforced Concrete, *Corrosion Review,* **20**, 129.

Bomberger et al. (1954) Corrosion Properties of Titanium in Marine Environments, *Journal of the Electrochemistry Society* **101**(9), 442-447.

Broendby (1999) Corrosion Aspects of Galvanic Coupling Between Carbon Steel and Stainless Steel in Concrete *Arminox Research and Development Report*, 2007.

Cochrane (1999) Efficient Use of Stainless Steel Reinforcement for Bridge Structure, *Infrastructure Regeneration and Rehabilitation Improving the Quality of Life Through Better Construction: A Vision for the Next Millennium*, (Swamy, editor), R.N. Sheffield Academic Press, Sheffield.

Cotton and Downing (1957) Corrosion Resistance of Titanium to Seawater, *Trans. Inst. Marine Engineering*, **69**(8), 311-319.

Gonzalez, J. A., Andrade, C., Alonso, C., & Feliu, S. (1995) Comparison of rates of general Corrosion and maximum pitting penetration on concrete embedded steel reinforcement. Mechanics of Composite Materials, 50(2), 257-264.

Gulikers and Schlangen (1996) Numerical analysis of galvanic interaction in reinforcement corrosion. *Corrosion of Reinforcement in Concrete Construction* (Page et al., editors), Royal Society of Chemistry.

Higgins, C. Knudtsen, J. Amneus, D. and Barker, L. (2017) Shear and Flexural Strengthening of Reinforced Concrete Beams with Titanium Alloy Bar, *Proceedings of the 2nd World Congress on Civil, Structural, and Environmental Engineering (CSEE'17)*, Barcelona, Spain, Apr. 2017.

Higgins, C. Amneus, D. and Barker, L. (2015) Methods for Strengthening Reinforced Concrete Bridge Girders Containing Poorly Detailed Flexural Steel Using Near-Surface Mounted Metallics, Report No. *FHWA-OR-RD-16-02*, Oregon Department of Transportation, Salem, OR, 138 pp.

Hope (2001) Some corrosion aspects of stainless steel reinforcement in concrete, *Final report* of MTO special project Q900076.

Klinghoffer et al. (2000) Practical and Economic Aspects of Application of Austenitic Stainless Steel, AISI 316, as Reinforcement in Concrete, *Corrosion of reinforcement in concrete: corrosion mechanisms and corrosion protection* (Mietz et al., editors).

Knudsen and Skovsgaard (2001) Stainless steel reinforcement, *Concrete Engineering*, **5**(3), 59.

Laque (1975) *Marine Corrosion: Causes and Prevention*, John Wiley and Sons, 332 pp.

Mangrat, P.S. and Elgarf, M.S. (1999) Flexural Strength of Concrete Beams with Corroding Reinforcement, *ACI Structural Journal* **96**(1), 149-158.

Nossoni, G., Harichandran, R.S. and Baiyasi, M.I. (2015) Rate of Reinforcement Corrosion and Stress Concentration in Concrete Columns Repaired with Bonded and Unbonded FRP Wraps, *ASCE Journal of Composites for Construction* **19**(5).

Pérez-Quiroz et al. (2008) Assessment of stainless steel reinforcement for concrete structures rehabilitation. *Journal of Constructional Steel Research* **64**(11), 1317-1324

Portland Cement Association (PCA) (1970) Corrosion of Nonferrous Metals in Contact with Concrete, *Modern Concrete*.

Poursaee, A. (2011). Corrosion Measurement Techniques in Steel Reinforced Concrete, *Journal of ASTM International* **8**(5), 1-15

Platt, S. (2018) *Development of Titanium Reinforcing Bars for Concrete and Masonry*, Doctoral dissertation, University of Pittsburgh.

Qu et al. (2003) Effects of galvanic coupling between carbon steel and stainless steel reinforcements. *NRCC 46634*, National Research Council of Canada, 27 pp.

Seibert, P.J. (1998). *Galvanic Corrosion Aspects of Stainless and Black Steel Reinforcement in Concrete*. (Master's thesis), Queen's University, Kingston, Ontario.

Song and Shayan (1998) Corrosion of steel in concrete: causes, detection and prediction, *ARRB Review Report 4*, Australian Road Research Board, 86 pp.

Webster (1997) A Discussion on Cell Action as It Refers to Steels in Concrete, *COR-97-7810-N*, CORRENG Consulting Service Inc., Downsview, Ontario, 1997.

Table 1 Galvanic corrosion test matrix.

152 x 152 x 152 mm concrete prisms having #4 A615 embedded bar	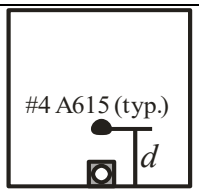	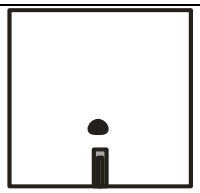	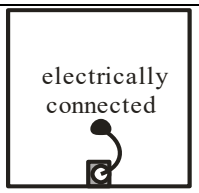	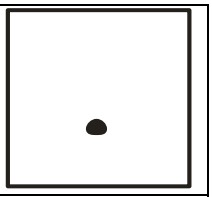
NSM Material	Ti, CFRP and SS	Tis	Ti, CFRP, SS & Tis	none
NSM dimension	12.7 mm dia.	25.4 x 5.1 mm	12.7 mm dia. & 25.4 x 5.1 mm	
area of NSM	129 mm^2	129 mm^2	129 mm^2	-
surface area of NSM	39.9 mm^2/mm	61 mm^2/mm	39.9 mm^2/mm & 61 mm^2/mm	
surface area ratio NSM:A615	1.0	≈1.5	1.0 & ≈1.5	-
d	51 and 102 mm	51 and 102 mm	electrically connected	-
NSM1: epoxy bonding agent	SIKADUR 30	SIKADUR 30	-	-
slot dimension	19 x 19 mm	38 x 12.7 mm	-	-
NSM2: cementitious bonding agent	SIKAGrout 212	SIKAGrout 212	-	-
slot dimension	19 x 19 mm	38 x 12.7 mm	-	-
NSM3: embedded in concrete	concrete	concrete	concrete	-
specimens	36 specimens	12 specimens	8 specimens	6 specimens

Table 2 Conditioning schedule.

Monday	Tuesday	Wednesday	Thursday	Friday	Saturday	Sunday
dry	wet	wet	dry	wet	wet	wet
tank uncovered, no heat, specimens permitted to dry	tank covered, heater engaged	tank covered, heater engaged	tank uncovered, no heat, specimens permitted to dry	tank covered, heater engaged	tank covered, heater engaged	tank covered, heater engaged

Table 3 Steel bar mass loss.

	average mass loss over 152 mm length					12.6 mm length	max pit
	n	average	COV	min	max	max pit mass loss	average
control	2	5.8%	0.12	5.3%	6.3%	16.5%	2.84
titanium bar	14	5.1%	0.46	1.9%	10.8%	18.6%	3.65
titanium strip	14	4.8%	0.27	2.5%	6.7%	16.0%	3.33
CFRP bar	14	5.3%	0.21	4.0%	7.2%	8.2%	1.55
stainless steel bar	14	6.2%	0.24	3.3%	8.1%	23.5%	3.79

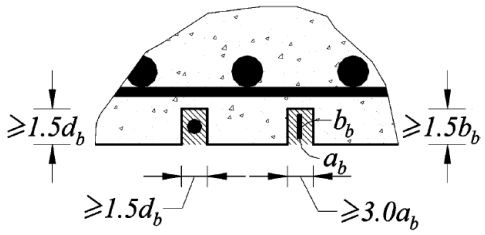

Figure 1 Minimum dimensions of NSM ‘slots’ (ACI 440.2R-17 Fig. 14.3).

a) plain and 'potted' NSM bars prior to being placed in concrete
left to right:

#4 ASTM A615 "black steel"
12.7 mm Ti bar
Ti bar embedded in epoxy
Ti bar embedded in cementitious grout
#4 CFRP bar
CFRP bar embedded in epoxy
CFRP bar embedded in cementitious grout
#4 SS bar
SS bar embedded in epoxy
SS bar embedded in cementitious grout
25.4 x 5.1 mm Ti strip
Ti strip embedded in epoxy
Ti strip embedded in cementitious grout

b) 152 mm cube specimens (d = 102 mm shown)

Figure 2 Specimens prior to conditioning.

a) support of specimens in GFRP rack

b) all specimens in tank

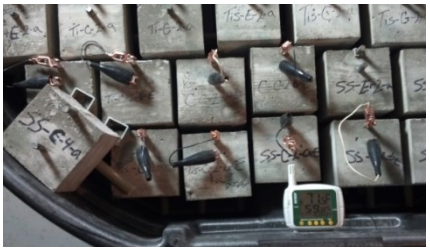

c) electrically coupled specimens and T/RH sensor

Figure 3 Specimens in conditioning tank (photo taken before conditioning begun).

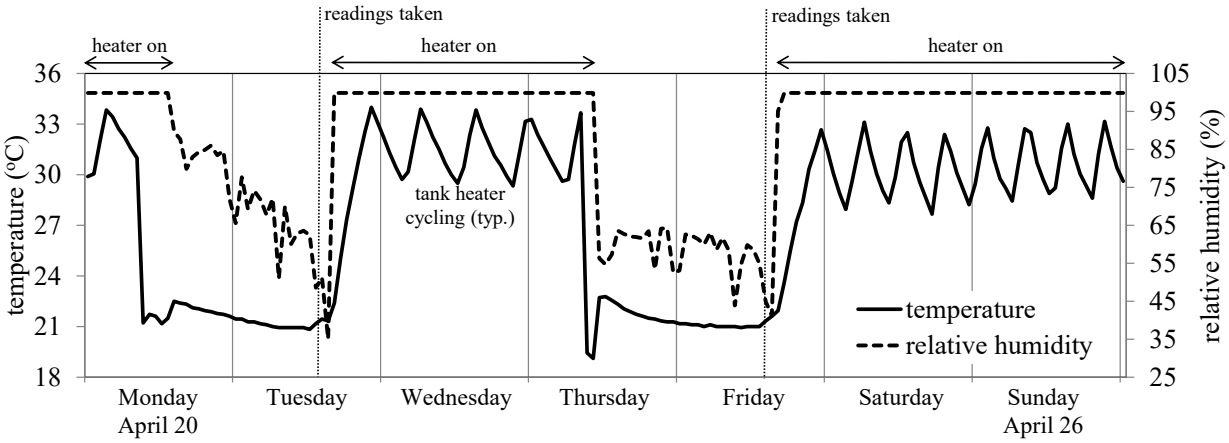

Figure 4 Typical weekly temperature/RH log.

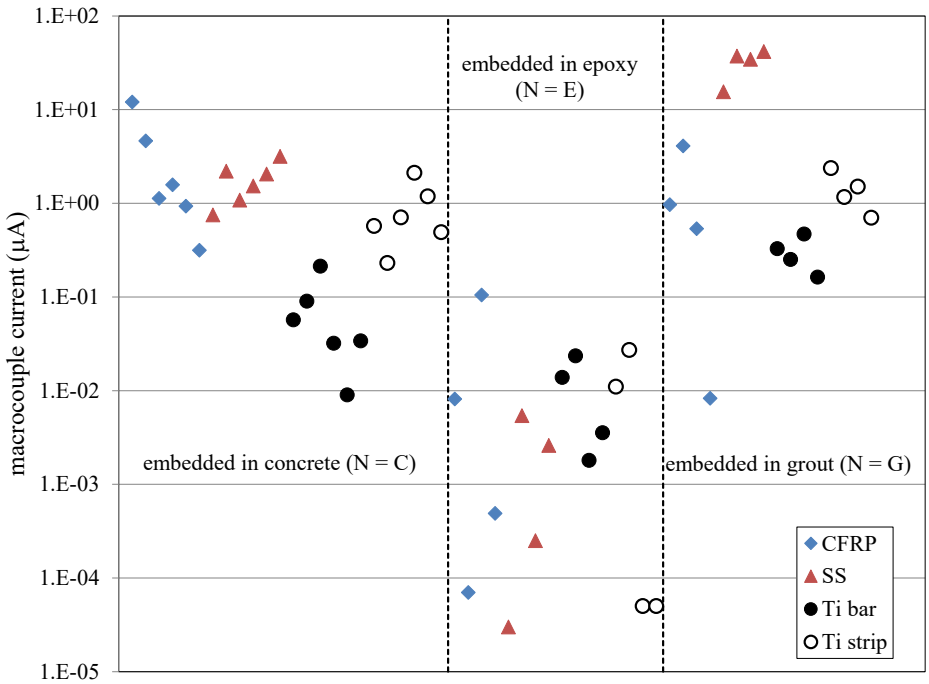

Figure 5 Grouping of specimens by macrocouple current prior to start of conditioning.

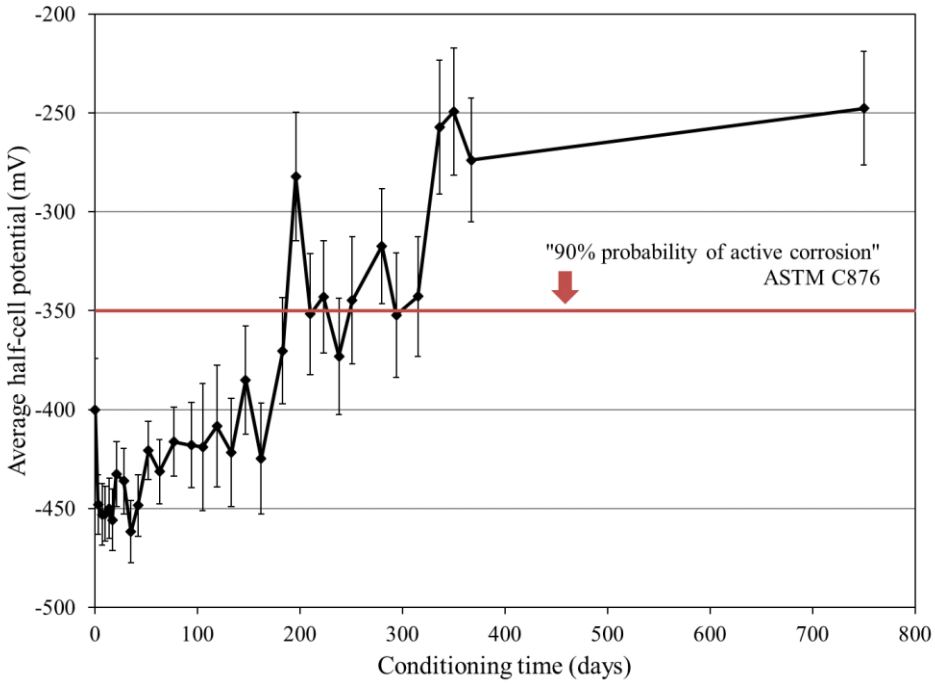

Figure 6 Half-cell potential history showing average and one standard deviation.

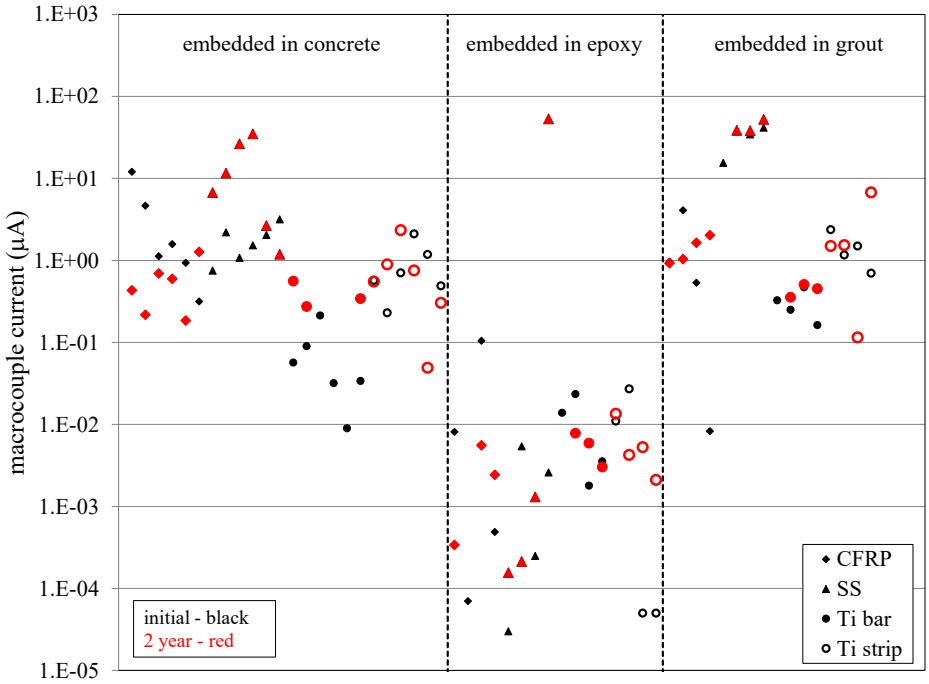

Figure 7 Macrocouple current following conditioning.

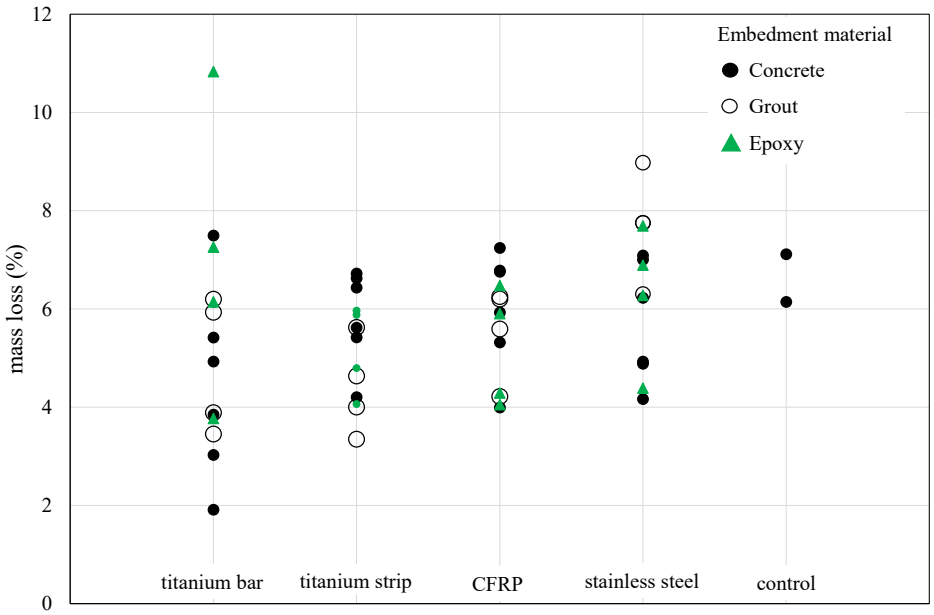

Figure 8 Average mass loss of embedded steel.